The 2012 World Congress on
Advances in Civil, Environmental, and Materials Research (ACEM' 12)
Seoul, Korea, August 26-30, 2012

LES Analysis of a Wind Turbine Wake Using an Actuator Disk Model

*Takaaki Kono[1)] and Tetsuya Kogaki[2)]

[1)] *Kanazawa University, Kakuma-machi, Kanazawa-shi, Ishikawa 920-1192, Japan*
[2)] *AIST, Namiki 1-2-1, Tsukuba-shi, Ibaraki 305-8564, Japan*
[1)] *t-kono@se.kanazawa-u.ac.jp*

ABSTRACT

This study investigated the influence of a wind turbine tower on wind velocity distribution in the wake of a wind turbine. Large-eddy simulation of the wind flow around the wind turbine was performed using an actuator disk model—which accounts for the thrust and tangential force acting on the rotating rotor—in (1) a case in which a wind turbine tower was explicitly resolved (Tower Case, TC) and (2) a case in which the effects of the tower were neglected (No Tower Case, NTC). Results confirmed that with regard to the streamwise component of the wind velocity in the wind turbine wake, TC reproduced the asymmetric distribution in the lateral direction observed in a wind tunnel experiment while NTC produced symmetric distribution. Visualization of the TC and NTC results suggested that the above-mentioned asymmetric wind velocity distribution predicted by TC were due to the enhanced turbulence and decreased velocity of wind flow behind the tower.

1. INTRODUCTION

When multiple wind turbines are deployed, it is important to assess the following two effects of the wakes of upwind wind turbines on downwind wind turbines. The first is reduced electric power generation caused by wind velocity reduction in the wakes of the upwind turbines, and the other is increased fatigue loading caused by increased turbulent fluctuations in the wakes of the upwind turbines (Manwell et al., 2009). Computational fluid dynamics (CFD) analysis is one method to evaluate these effects.
CFD analyses of the flow around a wind turbine can be classified roughly into 1) those which resolve turbine blades explicitly and 2) those which incorporate the force acting

[1)] Assistant Professor
[2)] Researcher

on the blades in the external force term of the Navier-Stokes equation (Sanderse et al. 2011). Because the former incur high computational costs, case examples of the former type of CFD analyses applied to wind turbine wakes are highly limited. On the other hand, case examples of the latter type of CFD analyses applied to wind farms as well as to individual wind turbines have been increasing in response to the development of models such as actuator disk (AD) models, in which the wind turbine rotor geometry is approximated as a disk, and actuator line (AL) models, in which the blade geometry is approximated as a line.

Some previous studies have examined the reproducibility of wind velocities in wind turbine wakes by CFD analyses which used AD or AL models. In these studies, the results of the CFD analyses were compared to wind tunnel experiment results. Major past research includes Cabezon et al. (2011), Porte-Agel et al. (2011), Uchida et al. (2011), Wu and Porte-Agel (2011), and Troldborg et al. (2010). All these studies investigated cases with upwind horizontal axis wind turbines. The authors of the present paper focus attention on the presence of the large asymmetry in the spanwise distribution of the wind velocity in the wind turbine wake at the hub height, a feature found in common among the wind tunnel experiment results reported in these studies. Although these studies neither discussed nor mentioned this asymmetry, Uchida et al. (2011) alone successfully reproduced this asymmetric tendency in a qualitative manner. In the CFD analysis of Uchida et al. (2011), the hub, nacelle, and wind turbine tower were resolved explicitly, which is considered a distinctive feature of this study. Although Porte-Agel et al. (2011) and Wu and Porte-Agel (2011) included forces exerted by the nacelle and wind turbine tower on the airflow in the external force term of the Navier-Stokes equation, these studies were unable to simulate the above-mentioned asymmetry as was the case for the other studies in the literature, which did not take into account the effects of the nacelle and tower. In addition, although the results were not compared to wind tunnel experiments, the CFD analysis of Uchida et al. (2010), which resolved only the hub (or more accurately, the spinner) explicitly and neglected the effect of the tower on the airflow, was not able to produce the above-mentioned asymmetry.

Based on the above, it can be speculated that the asymmetric spanwise distribution of the wind velocity in a wind turbine wake is attributable to the presence of a wind turbine tower. Therefore, the present study aims to verify the effects of a tower on the distribution of the wind velocity in a tower wake. For this purpose, a large eddy simulation (LES) is conducted with the use of an AD model for a case in which a tower is explicitly resolved and for a case in which the effects of the tower are neglected.

2. COMPUTATIONAL TECHNIQUE

In the present paper, a right-handed Cartesian coordinate system $(x_1, x_2, x_3) = (x, y, z)$ is used, in which the z-direction is aligned with the vertical direction, and incompressible fluid flows in neutrally stable atmospheric conditions are investigated. The simulation code utilized for analysis in the present study was developed based on the fluid dynamics simulation software FrontFlow/red (ver. 3.1.004) (Unemura et al. 2004).

2.1. Governing Equations and Discretization Method

The governing equations used in the study are the filtered continuity equation,

$$\frac{\partial u_i^g}{\partial x_i} = 0 \qquad (1)$$

and the filtered Navier-Stokes equation,

$$\frac{\partial u_i^g}{\partial t} + \frac{\partial u_i^g u_j^g}{\partial x_j} = -\frac{1}{\rho}\frac{\partial p^g}{\partial x_i} + 2\nu\frac{\partial S_{ij}}{\partial x_j} - \frac{\partial \tau_{ij}}{\partial x_j} + f_i \quad (2)$$

$$S_{ij} = \frac{1}{2}\left\{\frac{\partial u_i^g}{\partial x_j} + \frac{\partial u_j^g}{\partial x_i}\right\} \qquad (3)$$

$$\tau_{ij} = \{u_i u_j\}^g - u_i^g u_j^g \qquad (4)$$

where u_i is the wind velocity component in the x_i direction, p is pressure, ν is the kinematic viscosity, t is time, ρ is air density, f_i is the force exerted by the wind turbine rotor, and the superscript g indicates a quantity to which a grid-scale filter has been applied. The sub-grid scale (SGS) stress is calculated from the standard Smagorinsky model (Smagorinsky, 1991) as

$$\tau_{ij} = \{C_s f_v \Delta\}^2 \{2S_{ij}S_{ij}\}^{1/2} \qquad (5)$$

where C_s is the Smagorinsky constant, set to 0.1 in the present analysis, f_v is the van Driest damping function (Van Driest, 1956), and Δ is the computational grid scale.

The governing equations are spatially discretized on a collocated grid using the cell-vertex finite volume approach. In order to ensure numerical stability, the advection term is discretized using a first-order upwind difference scheme in the vicinity of the rotor (three grids upwind of the rotor and one grid downwind of the rotor) and a combined scheme consisting of a second-order central difference scheme (90%) and a first-order upwind difference scheme (10%) for the rest of the domain. The other terms are discretized using a second-order central difference scheme. For the computational algorithm, the SMAC method is utilized. Time integration is performed with the implicit Euler method.

2.2. Actuator Disk (AD) Model

Force exerted by the rotor, f_i, is calculated by an AD model based on the blade element theory described below.

Fig.1 illustrates the relationship among the relative wind velocity, V, the lift, dF_L, and the drag, dF_D, acting on a blade element, dr, located at a radial position along the blade measured from the rotor center, r. In this figure, the rotor plane is perpendicular to the streamwise direction, x. In this configuration, the following relationships hold:

$$V = \sqrt{u_1^2 + (r\omega - u_\theta)^2} \qquad (6)$$

$$u_\theta = \sqrt{u_2^2 + u_3^2} \qquad (7)$$

$$\alpha = \tan^{-1}\left(\frac{u_1}{r\omega - u_\theta}\right) - \gamma \qquad (8)$$

where c is the chord length, ω is the angular velocity, θ is the tangential direction, u_θ is the wind velocity in the θ-direction, α is the angle of attack, and γ is the blade setting angle.

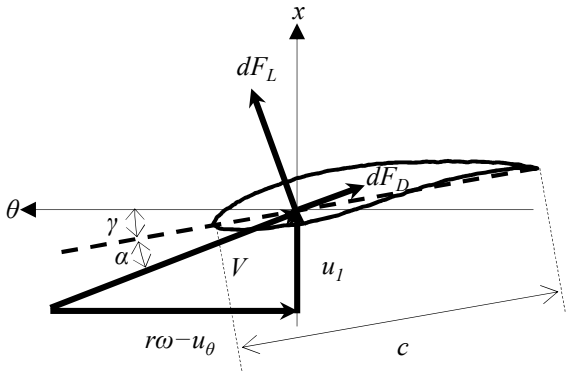

Fig.1 Relationship among the relative wind velocity, V, the lift, dF_L, and the drag, dF_D, acting on a blade element.

With the use of the lift coefficient, C_L, and drag coefficient, C_D, dF_L and dF_D acting on dr can be expressed as

$$dF_L = C_L \frac{1}{2}\rho V^2 c dr \qquad (9)$$

$$dF_D = C_D \frac{1}{2}\rho V^2 c dr\,. \qquad (10)$$

The thrust force, dF_x, and tangential force, dF_θ, can be expressed as

$$dF_x = dF_L \cos(\alpha+\gamma) + dF_D \sin(\alpha+\gamma) \qquad (11)$$

$$dF_\theta = dF_L \sin(\alpha+\gamma) - dF_D \cos(\alpha+\gamma)\,. \qquad (12)$$

If a rotor with radius R consists of B number of blades and is treated as a disk with a thickness of the computational grid width in the x-direction, Δ_x, the x- and θ-components of the body force, f_x, and f_θ, exerted on the fluid by the rotor at a radial position measured from the rotor center coinciding with the origin, r, can be expressed as

$$f_x = \begin{cases} -\dfrac{B}{2\pi r}\dfrac{dF_x}{\Delta_x dr}, & -\dfrac{\Delta_x}{2} \le x \le \dfrac{\Delta_x}{2},\ \ r \le R \\ 0, & \text{otherwise} \end{cases} \qquad (13)$$

$$f_\theta = \begin{cases} -\dfrac{B}{2\pi r}\dfrac{dF_\theta}{\Delta_x dr}, & -\dfrac{\Delta_x}{2} \le x \le \dfrac{\Delta_x}{2},\ \ r \le R \\ 0, & \text{otherwise} \end{cases} \qquad (14)$$

where $B/2\pi$ is the probability of a blade element being present at the point concerned. While the value of f_x is directly used for the x-component of the force exerted by the rotor, the value of f_θ is decomposed into y and z directions for the y- and z-components of the force exerted by the rotor for the analysis.

2.3. Numerical Setup

Numerical simulations are performed for one of the cases investigated in the wind tunnel experiments by Krogstad and Adaramola (2011), specifically, the case with a tip speed ratio of λ = 0.579, in which a notable asymmetry is evident in the spanwise distribution of the wind velocity in the wake.

Figs 2 and 3 show the computational domain and grids, respectively, for a simulation case in which the hub, nacelle, and tower are explicitly resolved (Tower Case; TC hereafter). The rotor diameter is D = 0.894 m, and the dimensions of the y-z cross section of the computational domain and the wind turbine are matched to those from the wind tunnel experiment of Krogstad and Adaramola (2011). The hub and nacelle are streamline forms, consisting of two semi-elliptical bodies and a cylinder. The tower is represented by four tiered cylinders of different diameters (Krogstad and Adaramola (2011), Krogstad and Lund (2012)). The hub height is 0.91D, and the distance from the hub, nacelle, and tower wall to the closest adjacent grid point is approximately 0.004D. In the vicinity of the rotor, O-type grids are used. The rotor is divided into 50 and 100 segments in the radial and θ directions, respectively, and Δ_x is approximately 0.006D. Outside the O-type grids, unstructured grids are used in the domain extending over $-0.62D \le x \le 0.84D$, $-0.78D \le y \le 0.78D$, and $-0.91D \le z \le 0.82D$. Outside this domain, rectangular parallelepiped grids are used. The total number of nodes in the computational domain is approximately 2.8 million.

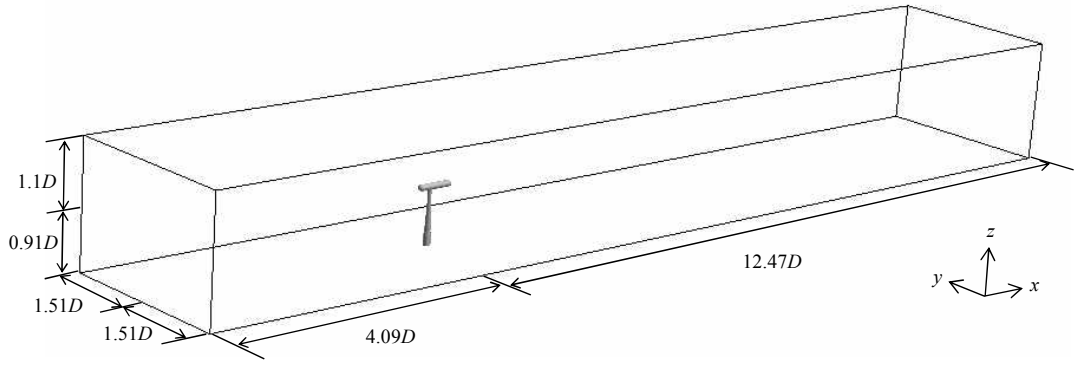

Fig.2 Computational domain (D: rotor diameter, 0.894 m)

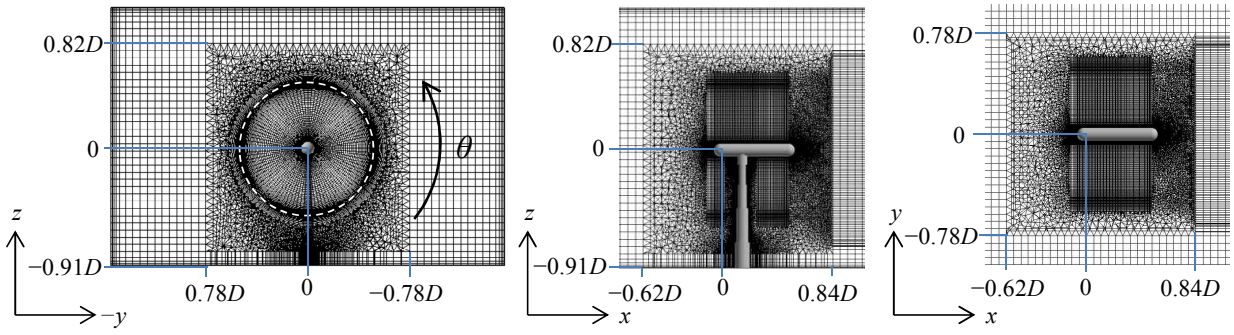

(a) y-z cross section at $x = 0$ (The white dotted line indicates the outer circumference of the rotor.)

(b) x-z cross section at $y = 0$

(c) x-y cross section at $z = 0$

Fig.3 Computational grids in the vicinity of the wind turbine (origin: rotor center)

Regarding the computational domain and grids used for the case which neglects the effects of the tower on the flow (No Tower Case; NTC hereafter), the dimensions of the computational domain are the same as those for TC. The computational grids are identical to those used in TC except in the vicinity of the tower. In the vicinity of the tower, the computational grids are symmetrical in the z direction with respect to the x-y cross section at z = 0, except in the vicinity of the ground surface. The total number of grid points in this case is approximately 2.6 million.

The rotor consists of three blades. The cross section of the blades is an NREL S826 airfoil (Somers, 2005) from the blade root to the blade tip. Fig.4 shows the distributions of c and γ as a function of the radial position (Krogstad and Lund (2012)). Because the values of V and c vary from the blade root to the blade tip, with the use of the airfoil analysis software Xflr5 (Deperrois, 2011), datasets of C_L and C_D are prepared for a range of α from -15° to 35° and a range of Reynolds number, Re_{Vc}, from 1×10^4 to 3×10^5 (Fig.5), where the Reynolds number is calculated based on V and c. Here, the data are created with an increment in Re_{Vc} of 1×10^4 up to Re_{Vc} = 1×10^5 and an increment of 1×10^5 for Re_{Vc} > 1×10^5. In Fig.5, only results from selected values of Re_{Vc} are shown for clarity. For high values of Re_{Vc} and α, the solution diverged, thus values of C_L and C_D were not obtained. However, this has no influence on the present study because Re_{Vc} only becomes as large as 1×10^5 and α only becomes as large as 10° even at the blade tip at which the maximum value of Re_{Vc} occurs.

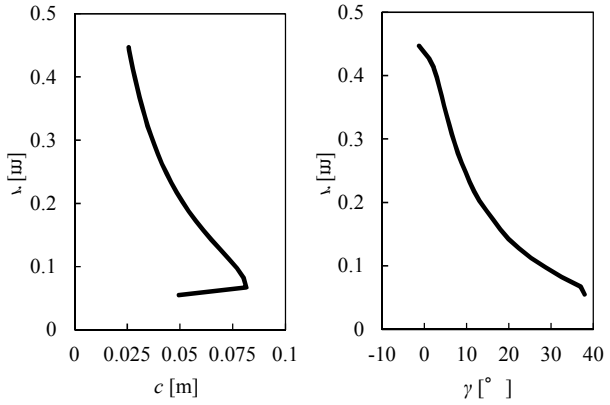

(a) Chord length (b) Pitch angle

Fig.4 Distribution of the blade chord length and pitch angle as a function of the radial position.

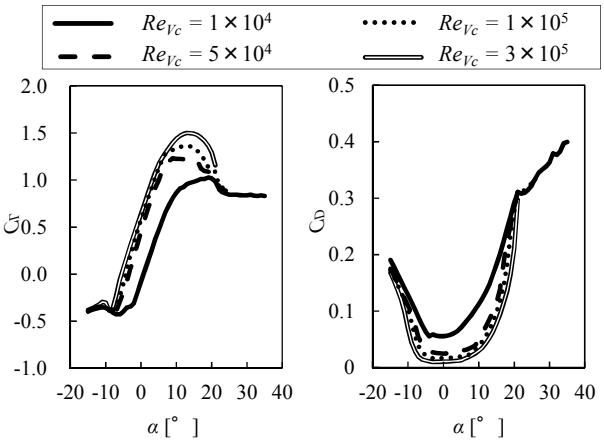

(a) Lift coefficient (b) Drag coefficient

Fig.5 Aerodynamic coefficients of the blades as calculated by Xflr5.

Table 1 shows the boundary conditions used in the model for velocity and pressure. The time-dependent turbulent inflow data that are provided at the inlet boundary are created in such a way as to match the turbulent intensity of the flow from the wind tunnel experiment (σ_u/U_∞ = 0.003). Specifically, turbulent flow is created by allowing uniform flow (wind velocity U_∞ = 10 m/s) to pass through a gird (Fig.6) and travel a distance of approximately 650D. Fig.7 shows the distributions of the mean wind velocity and turbulence intensity at the hub height at the inlet boundary. The figure also indicates the distribution of the hub-height turbulence intensity at x/D = 1 in the No Tower No Rotor Case (NTNR), which is the same as NTC except f_i = 0. Except in the

wake of the nacelle, the difference between the turbulence intensity at x/D = 1 and that at the inlet boundary is quite small. This implies that the influence on the turbulence in the inflowing wind of the numerical viscosity which arises from the first-order upwind difference scheme applied in the vicinity of the rotor is negligibly small.

Table 1 Boundary conditions for velocity and pressure

		Velocity	Pressure
Streamwise direction	Inlet x/D = –4.09	Time-dependent turbulent inflow (Fig. 7)	Neumann
	Outlet x/D = 12.47	Zero gradient	Neumann
Spanwise direction y/D = ±1.51		Logarithmic law for a smooth wall	Neumann
Vertical direction	Upper surface z/D = 1.1	Logarithmic law for a smooth wall	Neumann
	Lower surface z/D = –0.91	Logarithmic law for a smooth wall	Neumann
Hub, nacelle, tower		Logarithmic law for a smooth wall	Neumann

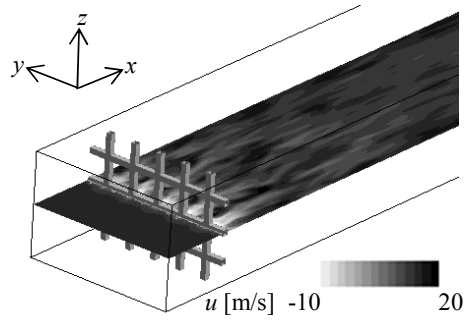

Fig.6 Generation of grid turbulence

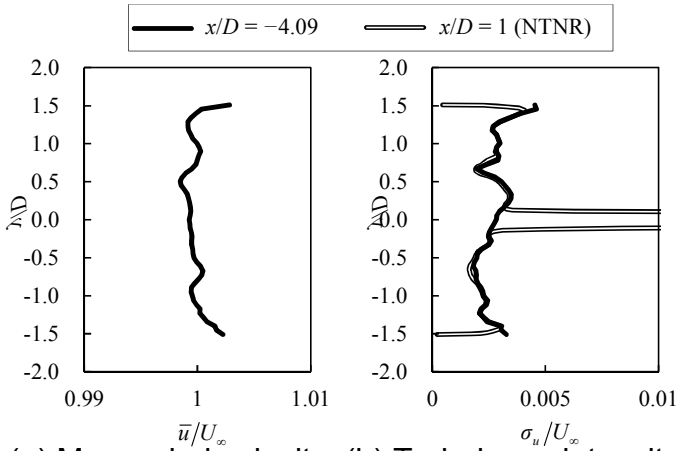

(a) Mean wind velocity (b) Turbulence intensity

Fig.7 Mean wind velocity and turbulence intensity of the time-dependent turbulent inflow at the hub height

For the simulations, the values of ν and ρ are set to those of air at 25°C, i.e., 1.54×10^{-5} m^2/s and1.184 kg/m^3, respectively. The Reynolds number based on U_∞ and D is approximately 5.8×10^5, and a time step interval of 2.5×10^{-4}s is adopted. The statistics of the flow are calculated over the time interval t = 5 - 25 s. The time-averaged value of an arbitrary physical quantity φ is indicated as $\overline{\varphi}$.

3. SIMULATION RESULTS AND DISCUSSIONS

3.1. Comparison of Simulation and Experiment Results

Table 2 shows a comparison of the values of the power coefficient, C_p, and the thrust coefficient, C_T, evaluated from the simulations to those from the wind tunnel experiments. C_p and C_T are defined as

$$C_P = \frac{-\omega \int_{-\frac{\Delta_x}{2}}^{\frac{\Delta_x}{2}} \int_{R_N}^{R} \int_0^{2\pi} f_\theta r^2 dx dr d\theta}{\frac{1}{2}\rho U_\infty^3 \pi R^2} \qquad (15)$$

$$C_T = \frac{-\int_{-\frac{\Delta_x}{2}}^{\frac{\Delta_x}{2}} \int_{R_N}^{R} \int_0^{2\pi} f_x r dx dr d\theta}{\frac{1}{2}\rho U_\infty^2 \pi R^2} \qquad (16)$$

where R_N is the radius of the nacelle. In TC, the deviations of the values of C_P and C_T from the simulations with respect to those from the experiments are 3% and 3.7%, respectively, suggesting that the simulation accurately reproduces the wind turbine performance. In NTC, the values of C_P and C_T are slightly larger than those in TC. The reason for this result may be that the volume of air flow passing through the rotor increases without the presence of a tower in NTC, suggesting that this result is qualitatively reasonable.

Table 2 Power and thrust coefficients

	C_P	C_T
TC （λ = 0.579）	0.450	0.828
NTC （λ = 0.579）	0.454	0.832
Wind tunnel experiment (Krogstad and Adaramola (2011)) (Linearly interpolated values for λ = 0.579 from the values evaluated at λ = 0.56 and 0.61)	0.437	0.860

Fig.8 shows comparisons between the simulation and wind tunnel experiment results (Krogstad and Adaramola (2011)) of the distribution in the y direction of $\overline{u}$ at the hub height in the wind turbine wake. While the symmetry in the y-direction, with respect to y = 0, is almost completely preserved for x/D = 1 – 4 in NTC, the symmetry is clearly absent in TC and the wind tunnel experiments. In comparison to the symmetrical distribution of $\overline{u}$ in NTC, asymmetry in the distribution of $\overline{u}$ in TC is clearly evident in the form of peak velocity deficits (Difference #1) in the vicinity of y/D = 0.1 for x/D = 1, in the vicinity of y/D = 0.2 for x/D = 2, and in the vicinity of y/D = 0.25 for x/D = 3. Asymmetry in TC is also evident in the form of a velocity recovery in the vicinity of y/D = 0.5 for x/D = 4 (Difference #2). In addition to these asymmetries, two other notable differences in the distribution of $\overline{u}$ between TC and NTC exist: a large velocity recovery in the vicinity of y/D = 0 for x/D = 1 – 4 in TC (Difference #3); and a large velocity deficit in the vicinity of y/D = ±0.1 for x/D = 3 – 4 in TC (Difference #4). Also, except for a limited area in the vicinity of y/D = 0 for x/D = 4, the difference in the distribution of $\overline{u}$ between TC and the wind tunnel experiments is smaller than that between NTC and the wind tunnel experiments. These results suggest that 1) a turbine tower has a significant

influence on the distribution of the wind velocity in the y-direction in the wind turbine wake and 2) appropriate inclusion and representation of a turbine tower is important for securing and improving the accuracy of simulated results.

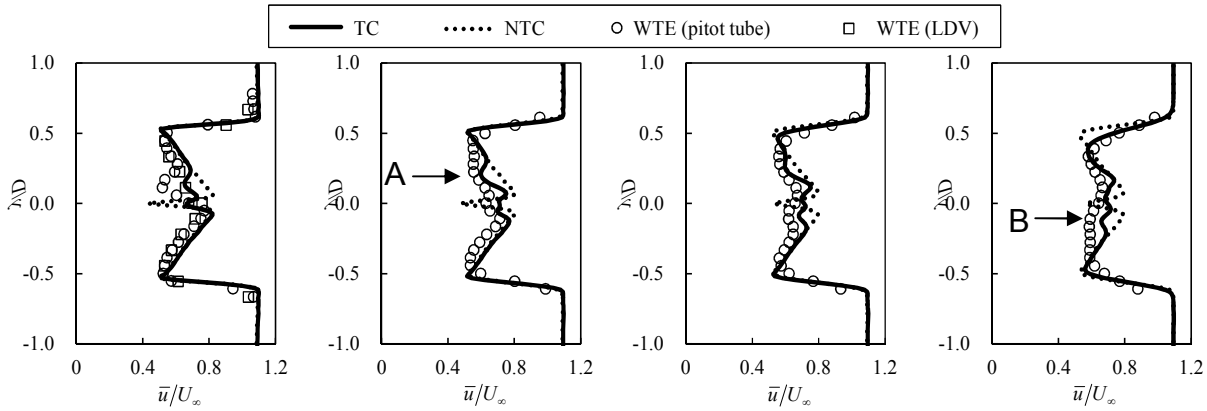

(a) x/D = 1 (b) x/D = 2 (c) x/D = 3 (d) x/D = 4

Fig.8 Spanwise distribution of the streamwise wind velocity at the hub height in the wind turbine wake. "WTE" represents the wind-tunnel experiments from Krogstad and Adaramola (2011).

3.2. Discussions Based on Visualizations of Simulation Results

In this sub-section, visualizations of the simulation results are used to examine the causes of the distinctive differences, Differences #1 - #4, in the distribution of wind velocity in the y-direction in the wind turbine wake between TC and NTC.

Figs 9, 10, and 11 are contour plots of the simulated values of u, $\overline{u}$, and turbulence kinetic energy, k, respectively, on horizontal and vertical cross-sections through the rotor center. The instantaneous as well as time-average fields of u over a broad area in the wind turbine wake are nearly symmetrical with respect to the x-axis in NTC (Figs 9 and 10). In addition, the values of k in NTC are significantly smaller than those in TC (Fig.11). On the other hand, in TC, turbulent fluctuations in the tower and nacelle wakes are particularly large. Also, turbulent fluctuations in the rotor wake on the $+y$ side are relatively large in this case. Comparisons of TC and NTC as displayed in these figures lead to the speculation that diffusion of momentum enhanced by the highly turbulent conditions in TC contributes significantly to the occurrence of Differences #1 – 4.

Subsequently, the reasons that the turbulent fluctuations in the wind turbine wake in TC are significantly larger than those in NTC will be examined. First, the occurrence of large turbulent fluctuations in the tower wake is fundamentally identical to that observed in the wake of a circular cylinder, thus, no further questioning is required on this point. Second, as for the cause of the occurrence of large turbulent fluctuations in the nacelle wake in TC in contrast to the significantly small turbulent fluctuations in the nacelle wake in NTC, the following speculation can be made: with the presence of a tower, the symmetry in the z-direction is lost for reasons including flow separation from the surface of the nacelle on the $-z$ side. Subsequently, separated vortices are shed from the downwind edge of the nacelle, which contributes to the large turbulent fluctuations in the nacelle wake in TC. Finally, the cause of the occurrence of large turbulent fluctuations on the $+y$ side of the rotor wake is examined. This phenomenon is

likely attributable to advection of the large turbulent fluctuations generated in the tower wake by the $-\theta$ rotational velocity component in the rotor wake, which forms in the opposite direction from the blade rotation. Fig.12 shows contours of k in y-z planes at x/D = 1 – 4 for TC. Large values of k generated in the tower wake at x/D = 1 are advected in the $-\theta$ direction with increasing values of x (Fig.12).

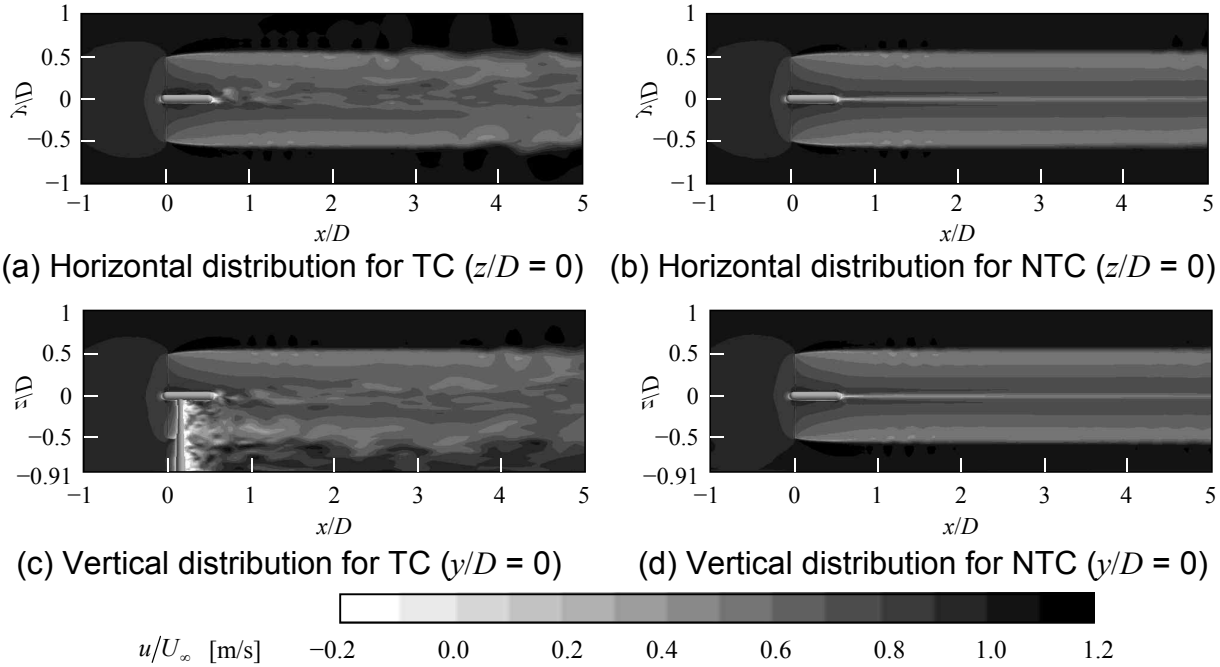

(a) Horizontal distribution for TC (z/D = 0) (b) Horizontal distribution for NTC (z/D = 0)

(c) Vertical distribution for TC (y/D = 0) (d) Vertical distribution for NTC (y/D = 0)

Fig.9 Contour plots of the instantaneous streamwise wind velocity (horizontal and vertical cross-sections through the rotor center)

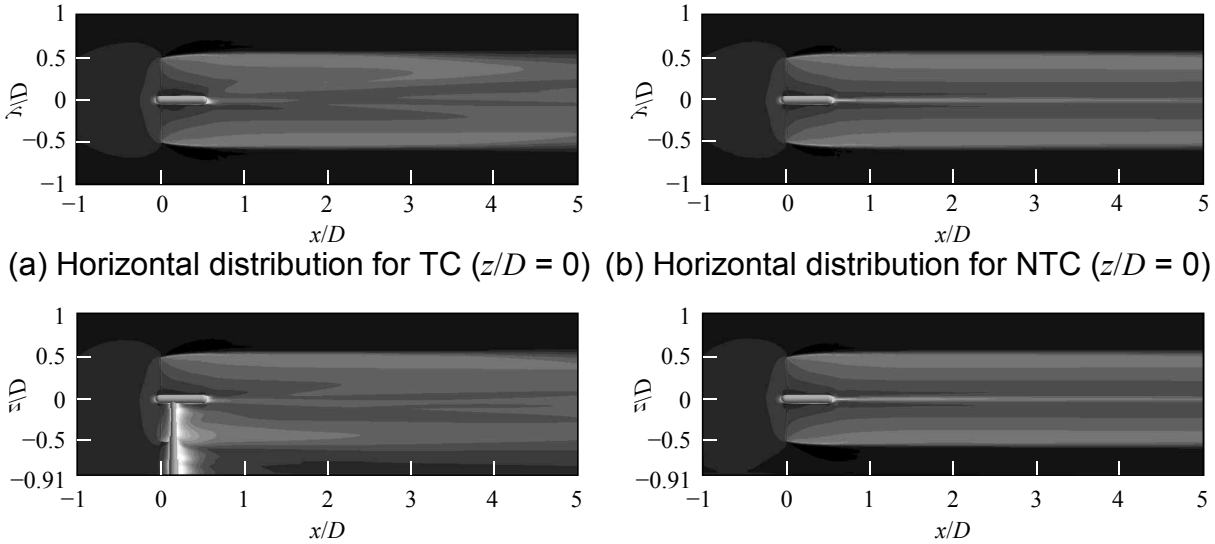

(a) Horizontal distribution for TC (z/D = 0) (b) Horizontal distribution for NTC (z/D = 0)

(c) Vertical distribution for TC (y/D = 0) (d) Vertical distribution for NTC (y/D = 0)

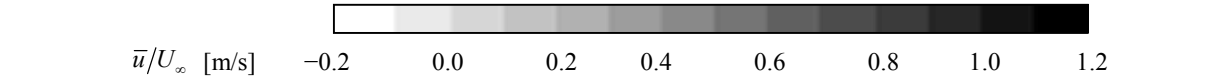

Fig.10 Contour plots of the time-averaged streamwise wind velocity (horizontal and vertical cross-sections through the rotor center)

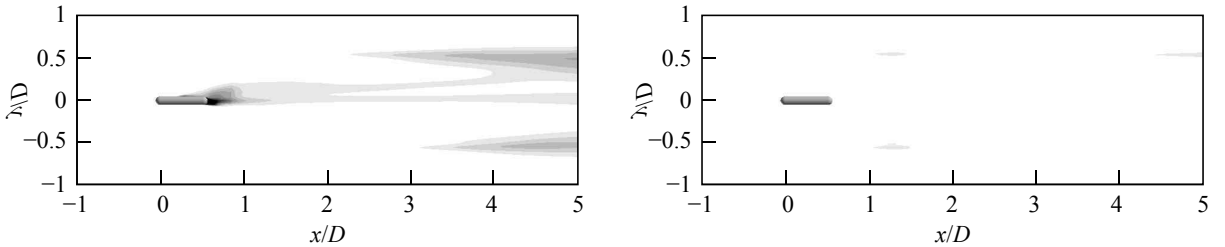

(a) Horizontal distribution for TC (z/D = 0) (b) Horizontal distribution for NTC (z/D = 0)

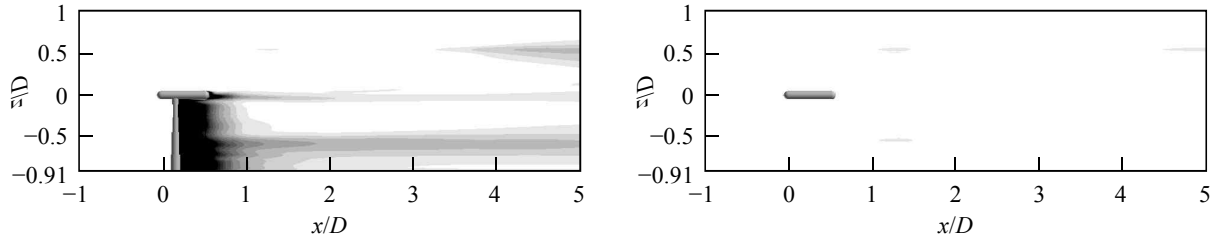

(c) Vertical distribution for TC (y/D = 0) (d) Vertical distribution for NTC (y/D = 0)

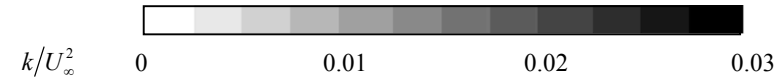

Fig.11 Contour plots of turbulence kinetic energy (horizontal and vertical cross-sections through the rotor center)

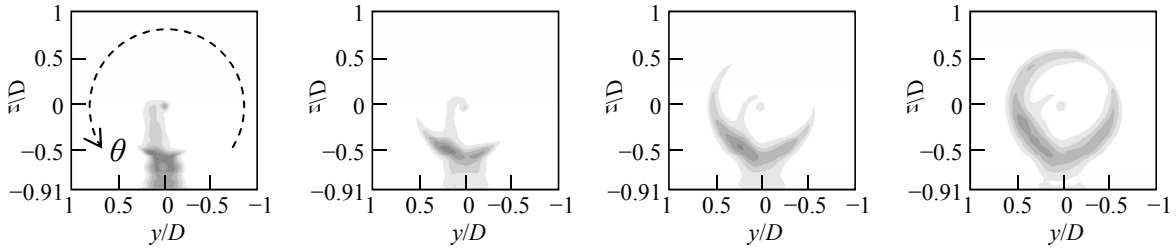

(a) x/D = 1 (b) x/D = 2 (c) x/D = 3 (d) x/D = 4

Fig.12 Contour plots of turbulence kinetic energy (y-z cross sections at x/D = 1 - 4 in TC)

The cause of the occurrence of Differences #1 and #4 cannot be sufficiently explained only by the enhancement of momentum diffusion by large turbulent fluctuations because local peaks of wind velocity reduction are present in the distributions in TC (Fig.8). Therefore, to investigate further, streamlines of the time-averaged flow are drawn which go through the vicinities of the local peaks in the $\overline{u}$ velocity reduction at x/D = 2 and x/D = 4, which are marked A and B in Fig.8, respectively (Fig.13). Fig.13 shows that the streamlines which go through the peaks of reduced $\overline{u}$ velocity A and B pass by the vicinity of the tower upwind of locations A and B. This result suggests that, in TC, which is reduced significantly in the tower wake in

the vicinity of the tower is advected by the $-\theta$ rotational velocity component in the rotor wake, contributing significantly to the occurrence of Differences #1 and #4.

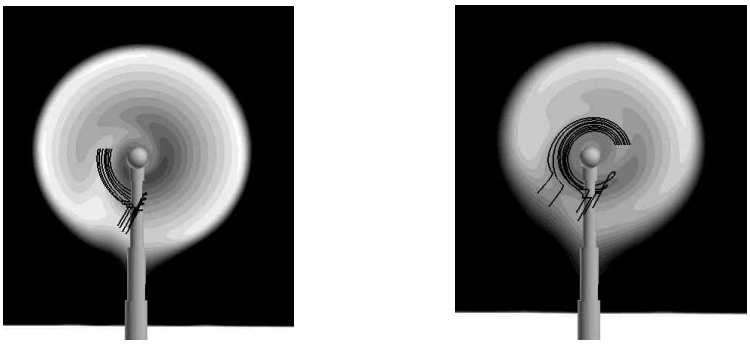

(a) Streamlines which go through the vicinity of the reduced velocity peak labeled A in Fig.8

(b) Streamlines which go through the vicinity of the reduced velocity peak labeled B in Fig.8

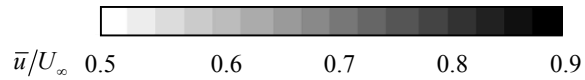

Fig.13 Streamlines of the time-averaged flow field (The y-z cross-sections of the velocity field for peaks A and B are those from x/D = 2 and 4, respectively, viewed from the –x direction toward the +x direction. For viewability, the left-hand side (+y) of the streamline plot has been tilted slightly in the +x direction and the right-hand side (-y) has been tilted slightly in the -x direction.

CONCLUSION

In the present study, large eddy simulations (LES) were performed with an actuator disk model in order to investigate the effects of a tower on the wind velocity distribution in the tower wake. For the simulations, two cases were considered: 1) a case in which a wind turbine tower was explicitly resolved (Tower Case, TC) and 2) a case in which the effects of the tower were neglected (No Tower Case, NTC). The findings from the analysis results are summarized below:

I. In TC, a notable asymmetry arose in the spanwise distribution of the time-averaged streamwise wind velocity in the wind turbine wake at the hub height. This asymmetry is similar to the asymmetry observed in a wind tunnel experiment (Krogstad and Adaramola (2011)). The set-up of the current LES analysis was designed to simulate the conditions of this wind tunnel experiment. Because of the asymmetry, the simulated results from TC are in better agreement with the wind tunnel experiment results than are the simulated results from NTC, which were characterized by a nearly symmetric distribution.

II. Two factors may contribute significantly to the differences in the spanwise distribution of the streamwise wind velocity in the wind turbine wake between TC and NTC: 1) enhancement of momentum diffusion caused by large turbulent fluctuations generated in the tower and nacelle wakes due to the presence of the tower and 2)

advection of significantly reduced wind velocity and large turbulent fluctuations in the tower wake by the rotational velocity component in the rotor wake that rotates in the opposite direction from the blade rotation.

From the findings above, it was confirmed that appropriate inclusion and representation of the tower are important for improving the accuracy of simulations of a wind turbine wake. Although it is ideal to explicitly resolve the tower configuration for improved simulation accuracy, in order to reduce computational costs, the effects of a tower on the airflow may be simulated by a drag model as in Porte-Agel et al. (2011). In this case, in order to increase the simulation accuracy, it is important to improve the model in such a way as to take into account the effects of the tower described in finding II above.

ACKNOWLEDGMENT

This research was partially supported by the project “Research and Development of Next-Generation Wind Power Generation Technology & Research and Development of Basic and Applied Technologies” of NEDO (New Energy and Industrial Technology Development Organization). The computation was mainly carried out using the computer facilities at Research Institute for Information Technology, Kyushu University.

REFERENCES

Cabezon, D., Migoya, E. and Crespo, A. (2011). “Comparison of turbulence models for the computational fluid dynamics simulation of wind turbine wakes in the atmospheric boundary layer,” *Wind Energy*, Vol. **14**, 909–921.

Deperrois, A. (2011). “Xflr5 v6.05 beta,” http://xflr5.sourceforge.net/xflr5.htm

Krogstad, P.A. and Adaramola M.S. (2011) “Performance and near wake measurements of a model horizontal axis wind turbine,” *Wind Energy*, doi: 10.1002/we.502

Krogstad, P.A. and Lund J.A. (2012). “An experimental and numerical study of the performance of a model turbine,” *Wind Energy*, **15**, 443–457. doi: 10.1002/we.482

Manwell, J.F. Mcgowan, J.G. and Rogers, A.L. (2009). “Wind energy explained theory, design and application,” *John Wiley & Sons Ltd.*, Second edition, 422.

Porte-Agel, F., Wu, Y.T., Lu, H. and Conzemius, R.J. (2011). “Large-eddy simulation of atmospheric boundary layer flow through wind turbines and wind farms,” *Journal of Wind Engineering and Industrial Aerodynamics*, Vol. **99**, 154–168.

Sanderse, B., van der Pijl, S.P. and Koren, B. (2011). “Review of computational fluid dynamics of wind turbine wake aerodynamics,” *Wind Energy*, Vol. **14**, 799–819.

Smagorinsky, J. (1991). “General circulation experiments with the primitive equations,” *Monthly Weather Review*, Vol.**91**(3), 99–164.

Somers, D.M. (2005). “The S825 and S826 Airfoils,” *National Renewable Energy Laboratory*, NREL/SR-500-36344.

Troldborg, N., Sorensen, J.N. and Mikkelsen, R. (2010) “Numerical simulations of wake characteristics of a wind turbine in uniform inflow,” *Wind Energy*, Vol. **13**, 86–99.

Uchida, T. and Ohya, Y. (2010). “Large-eddy simulation of the wake behind wind turbine generator under optimal tip speed ratio, –2nd report, Influence of inflow

turbulence generated by grid turbulence–," *Proceedings of the 21st National symposium on wind engineering*, 233–238. (in Japanese)
Uchida, T., Ohya, Y. and Sugitani, K. (2011). "Comparisons between the wake of a wind turbine generator operated at optimal tip speed ratio and the wake of a stationary disk," *Modelling and Simulation in Engineering*, Vol. **2011**, ID 749421.
Unemura, T., Zhang, H. and Taniguchi, N. (2004). "Development of the fluid dynamics simulation software "FrontFlow/Red"," Seisan Kenkyu, **56**, 40–43.
Van Driest, E. R. (1956). "On turbulent flow near a wall," *Journal of the Aeronautical Sciences*, Vol. **23**, 1007–1011.
Wu, Y.T. and Porte-Agel, F. (2011). "Large-eddy simulation of wind-turbine wakes: evaluation of turbine parametrisations," *Boundary-Layer Meteorology*, Vol. **138**, 345–366.